Journal of Inclusion Phenomena and Molecular Recognition in Chemistry **22:** 1–13, 1995.

Guest–Guest Interaction and Phase Transitions in the Natural Zeolite Laumontite

S. P. GABUDA and S. G. KOZLOVA
Institute of Inorganic Chemistry of Siberian Department, Russian Academy of Sciences, 630090 Novosibirsk, Russia.

(Received: 23 August 1994; in final form: 2 February 1995)

Abstract. The zeolite water arrangement in laumontite $Ca_{3.85}Na_{0.23}K_{0.06}Al_{7.96}Si_{16.03}O_{48} \cdot nH_2O$ (n = 16–18) and leonhardite (n = 12–14.4) has been studied from ^1H and ^{27}Al-NMR data at temperatures of 200–390 K. Close agreement is found between NMR data obtained for samples n = 12 and n = 18 and previous X-ray and neutron diffraction data. The H_2O arrangement in the powder sample with n = 14.4 and in a laumontite single crystal is represented by a combination of the H_2O arrangements in samples with n = 12 and n = 18 with increased orientational H_2O disordering. Concentration-type phase transitions are found in the single crystal and the n = 16 and n = 18 samples at 226 and 230 K, and orientational-type phase transitions are found in the sample with n = 14.4 at 230 K, and in the sample with n = 18 at 293 K. The smooth transformations into an orientationally disordered glassy state arrangement of H_2O in the zeolite channels is found in samples with n = 14.4, 16, and 18 at 300–330 and 305–315 K.

Key words: Laumontite, leonhardite, phase transformation, low-dimension glassy state, NMR spectroscopy.

1. Introduction

Zeolites, as the typical channel-type compounds with open porous structures, are a convenient model for the study of guest–guest interactions. The rigid alumino silicate framework of zeolites allows one to change the population of the channels in wide ranges of composition and of filling degree. The resulting phenomena, such as phase transitions due to the guest-guest interaction in zeolites are still not studied.

The spontaneous and reversible transformation of laumontite into leonhardite with variation of surrounding humidity is well known [1]. A series of X-ray [2–7] and neutron diffraction [8, 9] studies clarified the crystal structure of laumontite and revealed the 'highest degree of disorder of the water molecules' among zeolites well characterized by neutron diffraction [8]. But the structural mechanism of this disorder and of the zeolite water rearrangements at the laumontite $\rightleftharpoons$ leonhardite transformation is beyond the scope of the later experimental approaches.

In this paper we apply ^1H-NMR spectroscopy to the characterisation of H_2O–H_2O interaction in the zeolite pores, H_2O arrangement, dynamics, and disordering

phenomena in the zeolite water sublattice in laumontite and its particular dehydrated forms over a wide range of temperature and H_2O partial pressure. ^{27}Al-NMR spectroscopy was used for independent control of conjugated changes in the zeolite host framework during the transformations occuring in the guest water sublattice.

2. Experimental

Laumontite crystal samples from the Nidym River deposit (Siberian Platform, Russia) were used in this study. The unit cell parameters are $a = 14.90$; $b = 13.17$; $c = 7.55$ Å; $\beta = 111.5°$, and the averaged chemical analysis of the sample yielded the composition

$$Ca_{3.85}Na_{0.23}K_{0.06}Al_{7.96}Si_{16.03}O_{48} \cdot nH_2O.$$

The whole specimen was submerged in water for several weeks and subsequently used for the single crystal NMR study of fully hydrated laumontite. Because the laumontite single crystal disintegrates in air, only powder samples of the partially dehydrated laumontite were studied. The fully hydrated powder sample (S1) was submerged into water, and the partially dehydrated powder samples were kept in vessels with stabilised relative humidities of 91% (S2) and 15% (S3) at room temperature for several weeks. Sample S3 was used for the preparation of partially dehydrated forms of laumontite. Sample S4 was prepared from S3 by flushing it with dry nitrogen at 333 K for 2 h, and S5 was prepared by flushing S4 with dry nitrogen at 393 K for 2 h. ^{1}H and ^{27}Al-NMR spectra were recorded at a Larmor frequency 18 MHz for both nuclei at fixed temperatures ranging from 200 to 390 K, the temperature control being accurate to $\pm 1°$.

3. Results

3.1. Single Crystal Data

The room-temperature ^{1}H-NMR spectra at different orientations of the sample in an external magnetic field $\mathbf{B}_0$ are represented by pairs of lines symmetrically spaced relatively to $\mathbf{B}_0$. The angular dependence of the splitting between these lines can be described as:

$$\Delta B = 2b \sin^2 \Theta \cos 2\Phi \qquad (1)$$

where Θ is the angle between $\mathbf{B}_0$ and the 010 axis, Φ is the angle between the projection of $\mathbf{B}_0$ on the basal plane (010) and the axis 100, and the experimental parameter $\mathbf{b}$ is 2.1 ± 0.1 G. The angle settings are accurate to $\pm 3°$ in this relationship.

Generally, $\mathbf{b} = \mathbf{B} - \mathbf{B}_0$ is the local magnetic field created by the proton magnetic moment at the neighbouring proton site in H_2O. Parameter $\mathbf{b}$ can be regarded as a second-rank tensor [10] with main components: $\mathbf{b}_a = \pm 2.1$ G; $\mathbf{b}_b = 0$; $\mathbf{b}_{c'} =$

$\mp$ 2.1 G, where a, b, and $c' = c \sin \beta$ denotes the orientations along the axis of the laumontite unit cell.

The angular dependence (1) is unaffected by temperature variation between 275 and 370 K, but the parameter **b** decreases sharply at 335 K and its high-temperature value is 1.3 $\pm$ 0.1 G. Decrease of temperature is accompanied by a sharp reverse change of **b** to the initial value, but the transformation temperature is 320 K. The resolved doublet structure of the ^{1}H-NMR spectrum gradually disappears as the temperature is lowered below 275 K because of an increase of the spectrum components width.

3.2. Powder Data

Typical room-temperature ^{1}H-NMR spectra of all the different phases of the laumontite – leonhardite system are represented in Figure 1. The fine structure and forms of these spectra **F**(**b**) can be described by the convolution [11]:

$$\mathbf{F}(\mathbf{b}) = \int_{-\infty}^{\infty} \mathbf{f}(\mathbf{b}) \exp[-\sigma/(\mathbf{B} - \mathbf{B}^*)]^2 \, \mathrm{d}\mathbf{b}, \tag{2}$$

where σ is the individual spectral component broadening factor, and $\mathbf{B}^*$ is the value of **B**, relative to the centre of this component. The function **f**(**b**) is determined as follows [11, 12]:

$$\mathbf{f}(\mathbf{b}) = [(\mathbf{b}_x - \mathbf{b})(\mathbf{b}_y - \mathbf{b})]^{-1/2} \mathbf{K}[\eta(\mathbf{b} - \mathbf{b}_z)(\mathbf{b}_x - \mathbf{b})]^{1/2}$$

$$\text{for} \quad \mathbf{b}_z < \mathbf{b} < \mathbf{b}_x; \tag{3}$$

$$\mathbf{f}(\mathbf{b}) = [(\mathbf{b} - \mathbf{b}_z)(\mathbf{b}_x - \mathbf{b}_y)]^{-1/2} \mathbf{K}[\eta(\mathbf{b}_x - \mathbf{b})/(\mathbf{b} - \mathbf{b}_z)]^{1/2}$$

$$\text{for} \quad \mathbf{b}_y < \mathbf{b} < \mathbf{b}_x; \tag{4}$$

$$\mathbf{f}(\mathbf{b}) = \mathbf{0} \quad \text{for} \quad \mathbf{b}_z < \mathbf{b} < \mathbf{b}_y, \tag{5}$$

where **K**(...) is the total elliptic integral, $\eta = |(\mathbf{b}_x - \mathbf{b}_y)/\mathbf{b}_z|$ is the assymmetry parameter, $|\mathbf{b}_z| > |\mathbf{b}_y| > \mathbf{b}_x|$, and Tr$\mathbf{b}_k = 0$.

The values of the main components $\mathbf{b}_x$,$\mathbf{b}_y$, $\mathbf{b}_z$ and the broadening factors σ were determined by the trial-and-error method to minimize the difference between the recorded spectra (Figure 1) and the calculated ones. The solution of this problem is unambiguous for the well-resolved ^{1}H-NMR spectra of S5, S4, S4′, S3 and of the high temperature phases of S2 and S1. The room-temperature phases of S2 and S1 are characterized by high σ values ($\sigma \approx \mathbf{b}_y$), and hence, by unresolved ^{1}H-NMR spectra. In this case only one component $\mathbf{b}_y$ of the averaged local field tensor can be determined, whereas $\mathbf{b}_x$, $\mathbf{b}_z$, and σ are uncertain. The parameters obtained from all spectra are represented in Table I.

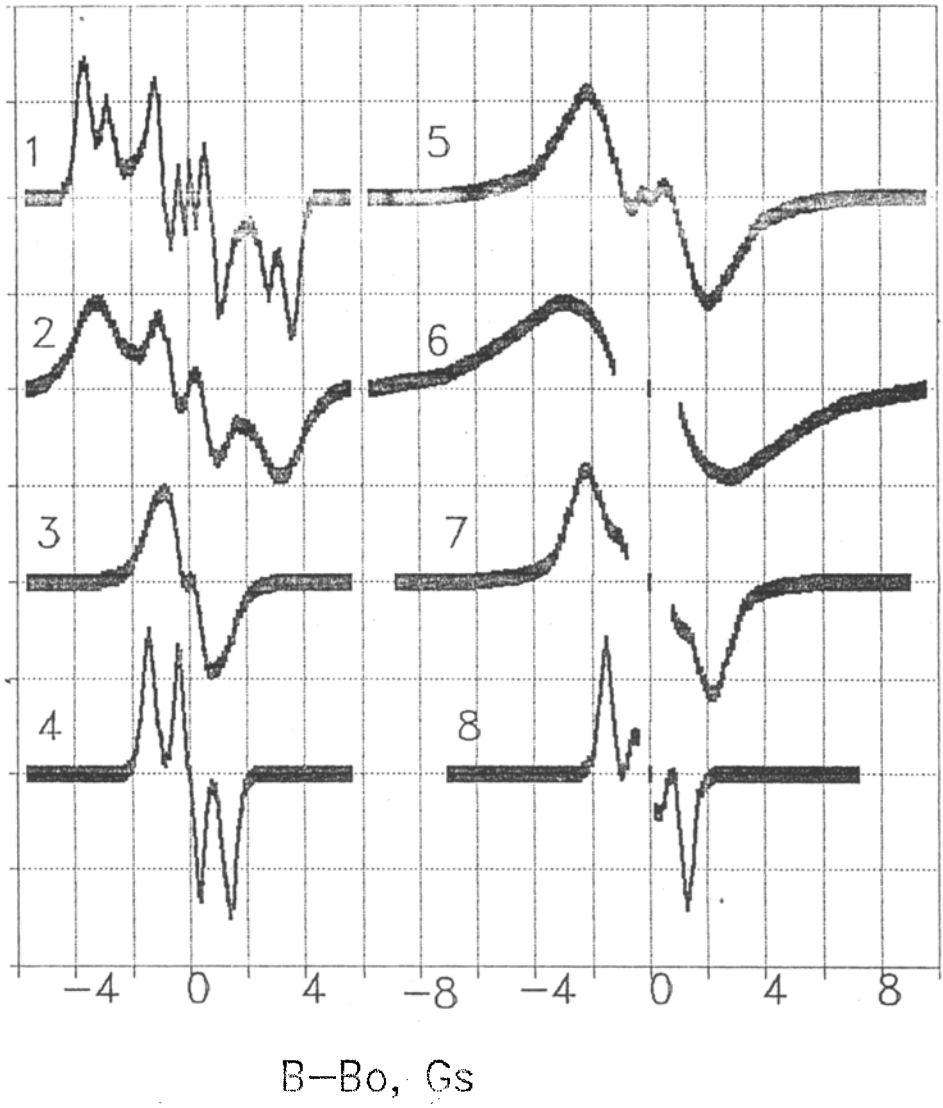

Fig. 1. ^{1}H-NMR spectra of partially dehydrated laumontite (1–5) and of laumontite immersed in water (6–8). Spectra (6–8) are represented without the strong central line of external water. 1 = S5 (390 K); 2 = S4 (330 K); 3 = S3 (290 K); 4 = S3 (360 K); 5 = S2 (290 K); 6 = S1 (290 K); 7 = S1 (310 K); 8 = S1 (360 K).

The temperature dependencies of $\mathbf{b}_y$ for all the studied samples are represented in Figures 2 and 3. It should be mentioned that the low-temperature (77 K) ^{1}H-NMR powder spectra of laumontite have been studied earlier [13]. The rigid zeolite water arrangement has been established and the interproton distance in the water molecules $\mathbf{R}$(H—H) = 1.58 Å has been measured. The rigid H_2O arrangement in laumontite gave way to a diffusion H_2O mobility at temperatures above 200–

TABLE I. ^{1}H-NMR parameters of different phases of the laumontite–leonhardite system.

Sample	$\mathbf{b}_x^*$, G	$\mathbf{b}_y^*$, G	$\mathbf{b}_z^*$, G	σ, G	n	T, K
S5	0.85	2.85	−3.70	0.1	10.8	240–390
S4	0.65	3.05	−3.70	0.2	11.6	243–333
S4′	0.58	3.17	−3.75	0.1	∼12**	293
S3	0.3	0.8	−1.1	0.2	14.4	233 ∼ 300
S3	0	1.3	−1.3	0.3	∼14.4	∼330–390
S2	–	2.2	–	0.8	∼16	275–326
S2	0	1.3	−1.3	0.3	∼16	∼330–390
S1	–	2.8	–	1.0	∼18	273–293
S1	–	2.2	–	0.7	∼18	293– ∼305
S1	0	2.1	−2.1	0.4	∼18	∼315–326
S1	0	1.3	−1.3	0.3	∼18	326–390

* Error limits are less than σ.
** Probable value for the sample, obtained by heating of S4 in open probe tube at 350 K (40 min).

270 K, that sharply narrows the ^{1}H-NMR spectra. Then the dependencies discussed above are related to the ^{1}H-NMR spectra recorded above the definite temperatures (240 K for samples S5, S4, S3; 270–280 K for samples S4 and S5), where the H_2O diffusion is fast enough to average the ^{1}H-NMR spectra.

The obtained $\mathbf{b}_y$ values of S5 and S4 are nearly constant at 240–390 K, whereas the temperature dependence of this parameter for S3 revealed an abrupt change at 230 K (phase transition into the low-temperature rigid state). The abrupt changes of $\mathbf{b}_y$ for S4 and S5 (Figure 3) take place at 293 and 326 K. The unusual smooth changes of $\mathbf{b}_y$ were found in S3 at 300–330 K (Figure 2) and in S5 at 305–315 K (Figure 3).

3.3. ^{27}Al-NMR Data

In the ^{27}Al-NMR study, only the central transition ($\frac{1}{2} \rightleftharpoons -\frac{1}{2}$ spin excitation) was measured. All registered spectra revealed a well-resolved fine structure caused by the second-order quadrupolar effects. The numerical analysis of spectra was performed according to the standard method [14]. The data obtained for the temperature dependence of the ^{27}Al quadrupolar interaction constant in laumontite (sample S1) are represented in Figure 4 together with the same data of partially dehydrated forms of laumontite. The asymmetry parameter [14] of the ^{27}Al quadrupolar coupling tensor of S1 was 0.9 below 326 K, and 0.6 above this temperature; for the samples S3, S4, and S5 the assymmetry parameter was temperature independent and equal to 0.5.

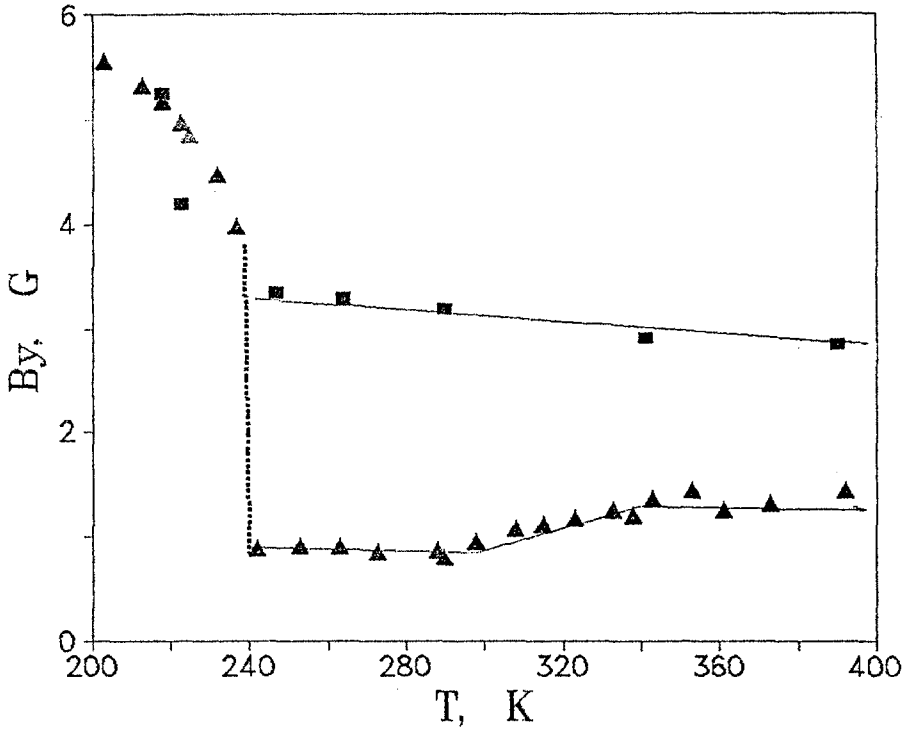

Fig. 2. The temperature dependencies of the component $\mathbf{b}_y$ of the ^{1}H dipolar interaction tensor for S5 (■) and S3 (▲). The vertical dashed line at the discontinuity point (233 K) indicates the phase transition.

4. Data Analysis

The diffusion averaged local magnetic field tensor components $\langle \mathbf{b}_k \rangle$ $(k = x, y, z)$ of narrow spectra are the crystal structure invariants, depending only on the hydrogen atom coordinates [11, 12]:

$$\langle \mathbf{b}_k \rangle = \pm 3/2\mu \mathbf{R}^{-3} \sum_{i=1}^{N} p_i [3\cos^2(\theta_{ik}) - 1], \tag{6}$$

Here μ is the proton magnetic moment, $\mathbf{R}$ = 1.58 Å [13], θ_{ik} is the angle between the definite crystal axis k and the H—H vector orientation of $(H_2O)_i$, and p_i is the population of site i, and N is the total number of sites with different θ_{ik}. The spread of θ_{ik} due to the H atoms' thermal motion (or disordering) can be taken into account as follows [12, 15]:

$$\langle \mathbf{b}_k \rangle_{\text{therm}} = \langle \mathbf{b}_k \rangle (1 - 2.52\langle \theta^2 \rangle), \tag{7}$$

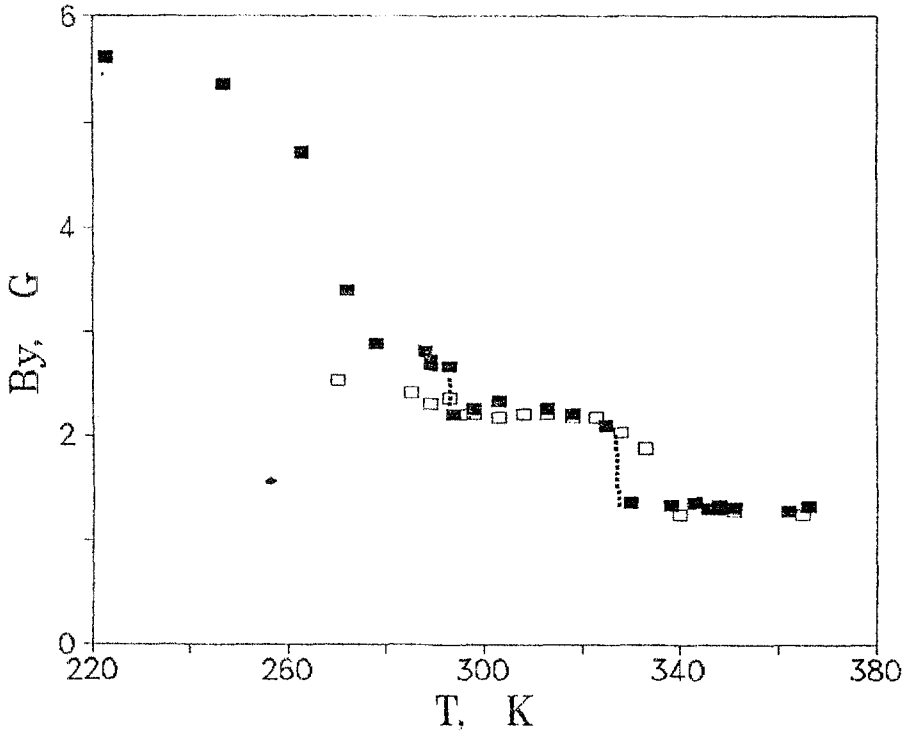

Fig. 3. The temperature dependence of the $\mathbf{b}_y$ component of the ^{1}H dipolar interaction tensor for S1 (■) and S2 (□). The vertical dashed lines at the discontinuity points (293 and 336 K) indicate the phase transitions.

where $\langle\theta^2\rangle$ is the root-mean-square angle of H—H vector librations. If the temperature factor coefficient B of the definite hydrogen atom is $B \ll \mathbf{R}^2$, then

$$\langle\theta_i^2\rangle \approx B/\mathbf{R}^2. \tag{8}$$

4.1. LEONHARDITE (12 WATER MOLECULES)

The calculation of $\langle\mathbf{b}_k\rangle$ can be done by using the structural data of leonhardite (12 water molecules) [4]. Starting with the H atom coordinates, we calculated the direction cosines of the H—H vectors of two water molecules O^{18} and O^{19} (Table II). The H—H vector direction of O^{19} was assumed to be along the b direction. Such an assumption complies with the location of O^{19} in a mirror plane. The interproton distance $\mathbf{R}$ = 1.58 Å was assumed for all H_2O_i sites. This $\mathbf{R}$ value is justified not only by the NMR data [13], but also by the fact that this value is the well established intramolecular distance of water molecules in crystal hydrates [12]. The calculated components are

$$\langle\mathbf{b}_a(\mathrm{S4}')\rangle = \mp 5.24\ \mathrm{G};\quad \langle\mathbf{b}_b(\mathrm{S4}')\rangle = \pm 0.48\ \mathrm{G};\quad \langle\mathbf{b}_{c'}(\mathrm{S4}')\rangle = \pm 4.76\ \mathrm{G}.$$

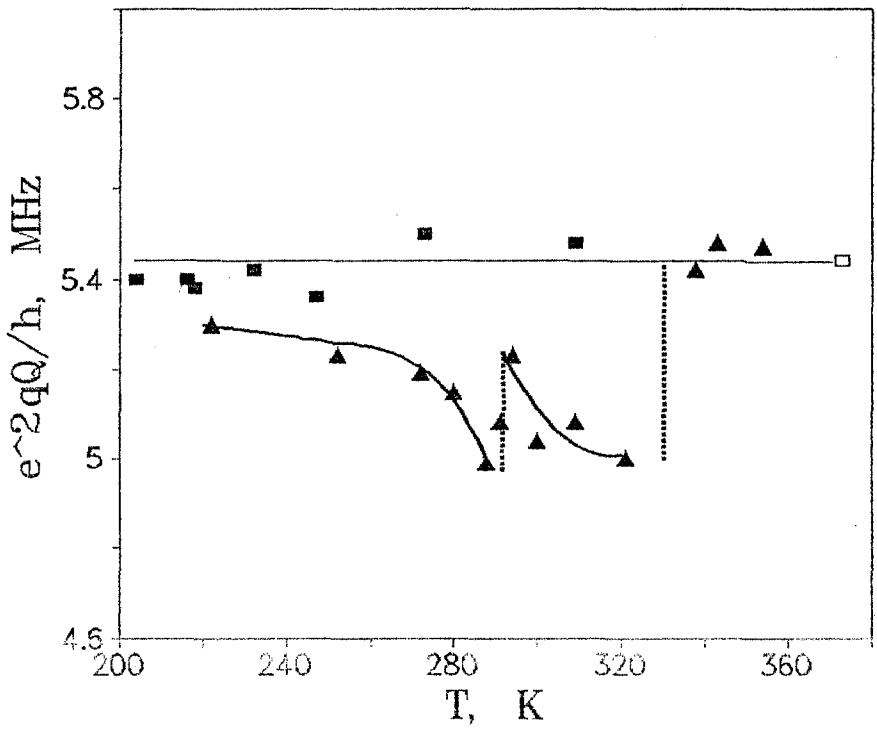

Fig. 4. The temperature dependencies of the ^{27}Al quadrupolar coupling constants e^2qQ/h in laumontite (S1, (▲)) and in leonhardite (S5 (□) and S3 (■)). The vertical dashed lines at the discontinuity points indicate the phase transitions.

TABLE II. H—H_i directional cosines in structures of leonhardite (n = 12) and of fully hydrated laumontite (n = 18).

i	O water	Vector	Population, $p(i)$	Cos θ_{ia}	Cos θ_{ib}	Cos θ_{ic}
Leonhardite [4]						
1	O19	H19-H19	1/3	0	1	0
2, 3	O18	H18-H18′	2/3	0.036	0.213	0.892
Laumontite [9]						
1	OW5	D5-D5	1/9	0.454	0	0.680
2	OW1	D1-D1	2/9	0.240	0	0.994
3	OW2	D21-D21	1/9	0	1	0
4	OW2	D21-D22	1/9	0.208	0.815	0.579
5	OW8	D81-D82	2/9	0.674	0.722	0.084
6	OW8	D82-D83	2/9	0.050	0.144	0.945

The orientation of the main axes of the calculated averaged dipolar tensor $\langle \mathbf{b}_k \rangle$ is exactly as in the laumontite single crystal. The specification of the orientations of main axes can be made on the basis of comparison of the calculated component values with the experimental data of samples S5, S4 and S4′ (Table I): x should be placed along b, y along $c' = c \sin \beta$, and z along a. The close accordance between the calculated and experimental tensor can be obtained, if we put $\langle \theta^2 \rangle = 0.12$ for all the H—H vectors.

A minor variation of the $\langle \mathbf{b}_k \rangle$ components of samples S4 (2.9 H_2O/Ca) and S5 (2.7 H_2O/Ca) relatively to sample S4′ (3 H_2O/Ca) can be explained by a slightly different change of the O^{18} and O^{19} [4] populations at partial dehydration of leonhardite with 12 water molecules in a unit cell.

4.2. Fully Hydrated Laumontite (18 Water Molecules)

The same calculations were made for the fully hydrated laumontite (18 water molecules) [9]. 6 directions D-D of 4 water molecules W(1, 2, 5 and 8) (Table II) were taken into account, and the main calculated components of the tensor are as follows:

$$\langle \mathbf{b}_a(\mathrm{S1}) \rangle = \mp 3.02 \text{ G}; \quad \langle \mathbf{b}_b(\mathrm{S1}) \rangle = \mp 0.44 \text{ G}; \quad \langle \mathbf{b}_{c'}(\mathrm{S1}) \rangle = \pm 3.46 \text{ G}.$$

The directions of the main axes of this tensor are exactly the same as in leonhardite (12 water molecules). The close accordance between the calculated and experimental $\langle \mathbf{b}_b \rangle$ component of sample S1 (below 293 K) can be obtained, if $\langle \theta^2 \rangle = 0.07$. The above tensor and $\langle \theta^2 \rangle$ parameters were used for simulation of the ^{1}H NMR spectrum. The coincidence of simulated and experimental spectra was achieved at σ = 1.6 G. The same analysis of samples S2 and S1 (above 293 K) data results in the same value $\langle \theta^2 \rangle = 0.13$, and σ = 1.2 G.

4.3. Partially Dehydrated Laumontite (14.4 Water Molecules)

The water molecules arrangement in S3 can probably be presumed to be a simple superposition of 60% of the arrangement in leonhardite (12 water molecules) and of 40% of the arrangement in fully hydrated laumontite (18 water molecules). The calculation of the main components of the averaged dipolar tensor in such structure is reduced to the linear combination of the two cases discussed above:

$$\langle \mathbf{b}_k(\mathrm{S3}) \rangle = 0.6 \langle \mathbf{b}_k(\mathrm{S4}') \rangle + 0.4 \langle \mathbf{b}_k(\mathrm{S1}) \rangle. \tag{9}$$

In such a model, the calculated components of the averaged dipolar tensor are as follows:

$$\langle \mathbf{b}_a(\mathrm{S3}) \rangle = \mp 4.35 \text{ G}; \quad \langle \mathbf{b}_b(\mathrm{S3}) \rangle = \pm 0.12 \text{ G}; \quad \langle \mathbf{b}_{c'}(\mathrm{S3}) \rangle = \pm 4.23 \text{ G}.$$

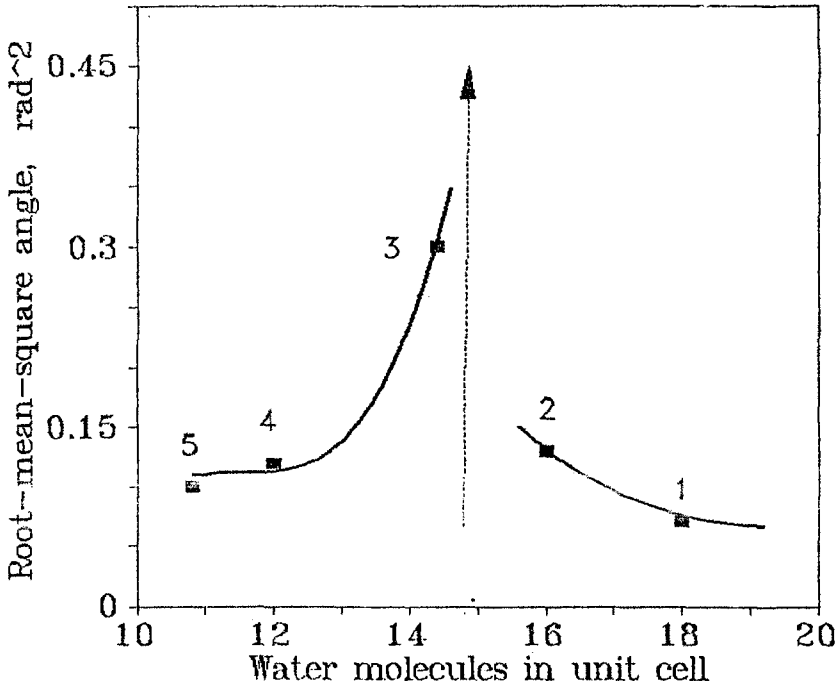

Fig. 5. The concentration dependence of the H_2O orientational disordering parameter $\langle\theta^2\rangle$ in laumontite samples S5–S1 (5–1). The arrow indicates the site completely disordered single crystal sample ($\langle\theta^2\rangle \approx \pi^2$).

The calculated components $\langle \mathbf{b}_{a,c'}(\mathrm{S3})\rangle$ are four times the experimental ones (Table I). In this case the orientational disordering parameter $\langle\theta^2\rangle = 0.3$. The increase of this parameter in S3 (Figure 5) is probably connected with the sharp increase of fluctuations of the parameter of ordering in the vicinity of the laumontite $\rightleftharpoons$ leonhardite phase transition.

4.4. Laumontite Single Crystal and High-Temperature Phases of Laumontite Powder

The calculation of the averaged dipolar tensor was done for the laumontite single crystal (14.2 water molecules in a unit cell) structure [8]. 45 H—H directions of water molecules located in 11 structurally different sites [8] were taken into account. The main components of tensor obtained are as follows:

$$\langle \mathbf{b}_{a''}(\mathrm{Sgl})\rangle = \mp 1.10\ \mathrm{G};\quad \langle \mathbf{b}_{b}(\mathrm{Sgl})\rangle = \mp 0.37\ \mathrm{G};\quad \langle \mathbf{b}_{c''}(\mathrm{Sgl})\rangle = \pm 1.47\ \mathrm{G}.$$

where a'' makes an angle $\phi = -14°$, and c'' makes an angle $\phi = 76°$ with the direction of the a axis. These directions deviate significantly from the observed ones, and the main axes values of this tensor are essentially less (by $\sim$2 times) than in the experiment. Such disagreement indicates that the low-temperature phase

transition takes place in laumontite, and the data [8] do not describe the room-temperature water molecules arrangement in a laumontite single crystal.

A definite conclusion about the water molecules arrangement in laumontite single crystal can be made from the direct analysis of its averaged H_2O diffusion dipolar tensor. The unusual feature of this tensor is the reducing to zero of its component $\mathbf{b}_b$. The powder samples S1, S2, and S3 demonstrate the same unusual feature, but only in their high-temperature phases (above 320 K).

Generally, the reduction of any component of the $\mathbf{b}_k$ tensor to zero indicates that a special arrangement of H—H vectors takes place. For example, if the H—H vectors in any structure forms the 'magic angle' (54°44′) with axis b, then, according to Equation (6), the corresponding component of the averaged dipolar tensor is reduced to zero. But it is improbable that such a special arrangement simultaneously occurs in 6 (see Table I) differently hydrated samples of the same zeolite.

The solution of the above problem consists in assuming, that $\langle\theta^2\rangle$ increases sharply and becomes more than π^2 in all the above discussed samples. In this case the spread of the H—H vectors orientations in each water site becomes spherically isotropic. In order to calculate $\mathbf{b}_b$ it is necessary to take into account that the isotropic average value of $\langle\cos^2\theta_{ik}\rangle_{av}$ is 1/3, and hence $\mathbf{b}_b = 0$.

4.5. Symmetry Consideration

According to the single crystal data (Equation (1)) the assumed isotropic spatial distributions of the orientations of H—H vectors is valid only relative to axis [010]. This fact can be connected with the influence of the polarising effect of the zeolite framework. The nature of such a polarising effect can be recognised on the basis of the laumontite structure [4–9] which is centrosymmetric in the space group $C2/m$. The zeolite channel axis 001 is lying in the structure mirror plane (010). Hence, the polarising influence of the laumontite framework on the isotropic distribution of orientations of water molecules has no dipolar constituents, and only the quadrupolar term of the polarisation of the same form as Equation (1) can exist.

The above symmetry consideration shows that polarisation induced by the laumontite framework is the only reason for partial deviations of the distribution of water molecules orientations from the isotropic one both in a single and in the high-temperature powder samples. This conclusion is consistent with the temperature independence of the $\mathbf{b}_b$ values outside the phase transition at 325–330 K. But there is no restrictions for the internal orientational ordering (even of ferroelectric type) of water molecules, if the temperature is lowered. The spontaneous ordering of molecular arrangement in channels can lead to $\mathbf{b}_b \neq 0$, and to the acentric space group both for low-temperature laumontite single crystal (below 275 K) and for powder S3, S2, and S1 (below 320 K).

5. Discussion

Theoretical considerations of phase diagrams in clathrate compounds [16, 17] shows that three types of phase transitions in such compounds are observed: orientational, concentrational, and induced. The ordering of guest-molecule orientations in a cavity or channel occurs at the phase transition of the first type. The 293 K phase transition in fully hydrated laumontite and the 230 K phase transition in partially dehydrated laumontite are probably of this type, because the observed sharp changes of ^{1}H-NMR spectra directly indicate the orientational ordering of certain water molecules in zeolite channels.

The smooth changes of ^{1}H-NMR spectra of fully hydrated laumontite at 305–315 K, and the same transformation in partially dehydrated laumontite at 300–330 K can also be referred to as transformations of the orientational type. But these transformations cannot be ascribed to the true phase transitions, because the occurence of high (rotational) local symmetry of any molecules in the crystal lattice do not change its symmetry [18]. Inasmuch as the high-temperature state of water in laumontite is orientationally (and positionally) disordered (according to ^{1}H-NMR data), this state can be regarded as a glassy state, and the discussed transformation can be regarded as melting of the ordered H_2O sublattice into a glass.

Other transformations in the laumontite-leonhardite system can be related to phase transitions of the concentrational type. Such transformations are characterized by a sudden exit of guest molecules from cavities or channels of a clathrate [17]. The 326 K transition in fully hydrated laumontite (powder sample) and the 330 K transition in laumontite single crystal definitely are of this type. Such a conclusion is warranted by an identity of the ^{1}H and ^{27}Al-NMR spectra of high-temperature phases of laumontite submerged in water, and of partially dehydrated laumontite (14 water molecules). The same conclusion was made previously [19] on the basis of an X-ray study.

The spontaneous laumontite $\rightleftharpoons$ leonhardite transformation at ambient conditions can also be regarded as of the concentrational type. But the important peculiarity of this transformation is the variation of the orientational ordering parameter (Figure 5) on change of hydration. By this is meant that the concentration phase transition in laumontite at ambient conditions is concerned with orientational disordering, and the transformation is of the mixed type. The combination of changes of H_2O concentration and of orientational ordering with influence of the crystal surface probably can explain the different structural behavior of laumontite single crystal and powder samples.

6. Conclusion

The above study shows that NMR spectroscopy of zeolites can be regarded as a significant supplement to structural investigations using diffraction methods. The

NMR method can be useful for independent determinations of interproton distances in crystals and as a criterium of reliability of complicated structure determinations from X-ray and neutron diffraction studies. The combination of proton magnetic resonance and diffraction methods can raise the level of insight into the complex problem of arrangement and disordering phenomena in guest sublattices and guest–guest interactions in zeolite pores.

Acknowledgements

We thank Professor G.N. Kirov and Dr. V.A. Drebushchak for supplying the samples. Financial support from the G. Soros International Science Foundation (grant number RBT000) and the Russian Fund for Fundamental Studies (project number 93-03-18231) is gratefully acknowledged.

References

1. D.S. Coombs: *Am. Mineral* **37**, 812 (1952).
2. S.T. Amirov, V.V. Ilyukhin, and N.V. Below: *Dokl. Akad. Nauk SSSR* **174**, 667 (1967).
3. O.V. Yakubovich and M.A. Simonov: *Kristallographiya* **30**, 1072 (1985).
4. T. Armbruster and T. Kohler: *N. Jb. Mineral Mh.* **H.9**, 385 (1992).
5. H. Bartl: *N. Jb. Miner. Mh.* 298 (1970).
6. A. Yamazaki, T. Shiraki, H. Nishido, and R. Otsuka: *Clay Science* **8**, 79 (1991).
7. G. Artioli and K. Stahl: *Zeolites* **13**, 249 (1993).
8. G. Artioli, J.V. Smith, and A. Kvick: *Zeolites* **9**, 377 (1989).
9. K. Stahl and G. Artioli: *Eur. J. Mineral.* **5**, 851 (1993).
10. S.P. Gabuda and A.G. Lundin: *Internal Mobility in Solids,* Nauka Press, Siberian Department, Novosibirsk (1986, in Russian).
11. N.A. Sergeev, O.V. Falaleev, and S.P. Gabuda: *Sov. Phys.-Solid State* **11**(8), 2248 (1969).
12. S.P. Gabuda and A.F. Rszavin: *Nuclear Magnetic Resonance in Crystal Hydrates,* Nauka Press, Siberian Department, Novosibirsk (1976, in Russian).
13. I.A. Belitsky, G.V. Bukin, S.P. Gabuda, and G.M. Mikhailov: *Dokl. Akad. Nauk SSSR* **159**, 1038 (1964).
14. J.F. Baugher, P.C. Taylor, T. Oja, and P.J. Bray: *J. Chem. Phys.* **50**, 4914 (1969).
15. B. Pedersen: *J. Chem. Phys.* **41**, 122 (1964).
16. J.H. van der Waals, and J.C. Platteeuw: *Adv. Chem. Phys.* **2**(1) (1959).
17. V.E. Zubkus, E.E. Tornau, and V.R. Belosludov: *Theoretic Physicochemical Problems of Clathrate Compounds.* In: I. Prigogine and S.A. Rice (Eds.): *Adv. Chem. Phys.* **79**, 269 (1992).
18. L.D. Landau and A.M. Lifshitz: *Statistical Physics,* Pergamon Press, Oxford (1967).
19. G.N. Kirov and I. Balkanov: *Geochem. Miner. Petr.* (Sofia) **4**, 57 (1975).